Title

The B56α subunit of PP2A is necessary for mesenchymal stem cell commitment to adipocyte

Journal

EMBO Reports, 22(8)

ISSN

1469-221X

Authors

Hanse, Eric A
Pan, Min
Liu, Wenzhu
et al.

Publication Date

2021-08-04

DOI

10.15252/embr.202051910

Peer reviewed

Article

SOURCE DATA | TRANSPARENT PROCESS

EMBO reports

The B56α subunit of PP2A is necessary for mesenchymal stem cell commitment to adipocyte

Eric A Hanse[1,†], Min Pan[2,†], Wenzhu Liu[1], Ying Yang[1], Mari B Ishak Gabra[1], Thai Q Tran[1], Xazmin H Lowman[1], Bryan Ruiz[1], Qiong A Wang[3] & Mei Kong[1,*]

Abstract

Adipose tissue plays a major role in maintaining organismal metabolic equilibrium. Control over the fate decision from mesenchymal stem cells (MSCs) to adipocyte differentiation involves coordinated command of phosphorylation. Protein phosphatase 2A plays an important role in Wnt pathway and adipocyte development, yet how PP2A complexes actively respond to adipocyte differentiation signals and acquire specificity in the face of the promiscuous activity of its catalytic subunit remains unknown. Here, we report the PP2A phosphatase B subunit B56α is specifically induced during adipocyte differentiation and mediates PP2A to dephosphorylate GSK3β, thereby blocking Wnt activity and driving adipocyte differentiation. Using an inducible B56α knock-out mouse, we further demonstrate that B56α is essential for gonadal adipose tissue development *in vivo* and required for the fate decision of adipocytes over osteoblasts. Moreover, we show B56α expression is driven by the adipocyte transcription factor PPARγ thereby establishing a novel link between PPARγ signaling and Wnt blockade. Overall, our results reveal B56α is a necessary part of the machinery dictating the transition from pre-adipocyte to mature adipocyte and provide fundamental insights into how PP2A complex specifically and actively regulates unique signaling pathway in biology.

Keywords adipocyte; B56α; PP2A; PPARγ; Wnt
Subject Categories Development; Metabolism; Signal Transduction
DOI 10.15252/embr.202051910 | Received 15 October 2020 | Revised 13 May 2021 | Accepted 27 May 2021 | Published online 7 July 2021
EMBO Reports (2021) 22: e51910

Introduction

The PP2A phosphatase plays an important role in a variety of tissues and cells removing phosphorylation moieties from substrate proteins during signaling cascades. As such, contextual control of PP2A activity is critical to normal cellular function. Not surprisingly, PP2A dysregulation is implicated in several diseases (Janssens & Goris, 2001; Eichhorn *et al*, 2009; Sangodkar *et al*, 2016). The PP2A holoenzyme consists of the structural scaffold A subunit, the catalytic C subunit, and the variable B subunit (Shi, 2009). The B subunit conveys specificity and directs the catalytic C subunit to its target for de-phosphorylation (reviewed in (Virshup & Shenolikar, 2009)). These fourteen B subunits are diverse in size and domain architecture. However, they are highly conserved in eukaryotes and coded by different genes scattered throughout the genome. B subunit expression is generally regulated transcriptionally and based on tissue- and context-dependent cues (Reid *et al*, 2013; Seshacharyulu *et al*, 2013). Genetic deletion of the PP2A C or other B subunits causes a variety of embryonic defects, suggesting an important role for PP2A in cellular development (reviewed in (Gotz & Schild, 2003)). Better understanding of B subunit specificity unlocks a whole new avenue of therapeutic targets with the potential to rival the success kinase inhibitors have had in the clinic.

Obesity rates are rising throughout the world (Collaboration NCDRF, 2019), and understanding the complex biology involved during the development and maintenance of adipose tissue is critical as we combat the accompanying complications arising from increased body fat mass (Kusminski *et al*, 2016). Prolonged overnutrition initiates the recruitment of nascent pre-adipocytes from local vasculature, which in turn expands to accommodate lipid storage demands. As pre-adipocytes differentiate into adipocytes, an orchestrated intracellular signaling cascade transduces extracellular cues into phenotypic changes via a currency of phosphorylation. Elucidating the kinase and phosphatase balance during this time is critical to understanding adipocyte development. We thus became interested in exploring B subunit expression and PP2A phosphatase activity during adipocyte development.

Here, we report the PP2A phosphatase plays a critical role in mediating the fate differentiation of adipocytes. Specifically, we show the PP2A-B subunit B56α is necessary for adipocyte differentiation. Using a novel mouse model, we establish B56α is necessary for the development of the gonadal white adipose tissue depot *in vivo*. We report that B56α is specifically induced upon adipocyte differentiation and correlates with GSK3β de-phosphorylation and Wnt signaling blockade during adipocyte development. Finally, we

1 Department of Molecular Biology and Biochemistry, University of California, Irvine, Irvine, CA, USA
2 Department of Computational Biology, St. Jude Medical Center, Memphis, TN, USA
3 Department of Molecular Endocrinology, Diabetes and Metabolism Institute, City of Hope Medical Center, Duarte, CA, USA
*Corresponding author. Tel: +1 949 824 5244; E-mail: meik1@uci.edu
†These authors contributed equally to this work.

show B56α is a PPARγ target gene, thereby establishing a mechanism for PPARγ-driven Wnt blockade. Our results uncover a critical signaling axis during adipocyte differentiation connecting PPARγ to the control of the Wnt pathway through the relationship between PP2A and GSK3β.

Results

The PP2A-B subunit, B56α, is required for adipocyte differentiation *in vitro*

The PP2A holoenzyme is directed to target substrate proteins by the specificity provided through its B subunits (Virshup & Shenolikar, 2009). The B subunits are encoded by genes across the chromosomal landscape, and their expression is context- and tissue-dependent (Gotz & Schild, 2003; Seshacharyulu *et al*, 2013). We initiated adipocyte development in the 3T3-L1 mouse pre-adipocyte cell line and in primary mesenchymal stem cells isolated from the outer ear of mice which differentiate to adipocytes under similar culture conditions (Rim *et al*, 2005). We then measured a panel of known B subunit genes for mRNA expression via RT–PCR to see whether any specific B subunits played a role during adipocyte development. We looked at day 6 when insulin maintenance has been established and adipogenic factors and morphology start to emerge. Among all the B subunits tested, we found the B56α subunit encoded by the *Ppp2r5a* gene was the only subunit significantly induced both transcriptionally and translationally in both 3T3-L1 and primary EMSCs, suggesting it may play a role in controlling phosphorylation during this process (Fig 1A–D). We next observed expression of the B56α protein during a time course and found B56α increased from day 2 until a maximal expression at day 6, which correlates with adipocyte differentiation markers (Figs 1E and F, and EV1A and B). Moreover, knock-down of B56α using shRNA significantly decreased the ability of 3T3-L1 and EMSCs to differentiate into adipocytes measured by Oil Red O, a stain for lipid storage (Fig 1G–J).

The PP2A-B subunit, B56α, is required for adipocyte differentiation *in vivo*

To examine whether B56α plays a significant role in the development of adipose tissue *in vivo*, we generated mice homozygous for a floxed exon 5 of the *Ppp2r5a* gene (Fig 2A). Primary EMSCs from these mice did not express B56α protein upon infection with a Cre recombinase expressing lentivirus, demonstrating knock-out (Fig 2B). We first attempted to cross these mice with adipose-specific Cre expressing mice Adipoq-CRE and observed no phenotypical change (Fig EV2A and B). We also crossed the $Ppp2r5a^{fl/fl}$ mice with FABP4-Cre and again observed no impact on adipose development. These data suggest the fate decision influenced by *Ppp2r5a* in adipocytes occurs prior to the differentiation required for expression of Adipoq and Fabp4. To better understand the adipose differentiation process influenced by B56α, we bred $Ppp2r5a^{fl/fl}$ mice to Rosa26Cre-ERT2 mice to produce a conditional whole-body knock-out. This model allows us to control *Ppp2r5a* expression prior to fat pad development. Most fat pads are established *in utero* or immediately after birth (Berry *et al*, 2013). Surprisingly, and in contrast to studies where Ppp2r5a has successfully been knocked out in a whole-body system (Janghorban *et al*, 2017), attempts to knock out *Ppp2r5a* during these time frames were lethal. These data suggest *Ppp2r5a* may play a role that is essential for development in adipose or other tissues, at least acutely. However, the gonadal white adipose tissue fat pad (gWAT) rapidly expands after day 21 as the mouse approaches sexual maturity (Berry *et al*, 2013). This allowed us a window to investigate the development of an isolated adipose depot. Thus, we injected tamoxifen at 21 days of age intraperitoneally 4 times over the course of a week into WT and $Ppp2r5a^{fl/fl}$ mice and allowed them to mature for an additional 4 weeks (Fig 2C). As previously reported, tamoxifen treatment alone slowed adipose tissue development ((Ye *et al*, 2015), Fig 2D). We found mice without *Ppp2r5a* had a significantly smaller gWAT depot than control mice treated with tamoxifen (Fig 2D–F) and exhibited dense cellularity observed by H&E staining, particularly around the tissue edges (Fig 2G). We did not observe gross histological differences in body mass nor in tissues such as subcutaneous WAT, brown fat or liver (Fig EV2C–E). Although the gWAT tissue was smaller in $Ppp2r5a^{fl/fl}$ mice treated with tamoxifen, average cell area was not significantly different among conditions (Fig EV2F). Moreover, adipose tissue depots established earlier in development such as subcutaneous WAT were not affected by loss of *Ppp2r5a* consistent with the idea that this signaling pathway is particularly important during adipose development (Fig EV2G). Taken together, these data demonstrate a critical role for the *Ppp2r5a* gene during the initiation of adipocyte differentiation and adipose tissue.

B56α binds to Axin1 and GSK3β during adipocyte development

The canonical function for PP2A as a phosphatase led us to ask what potential substrate proteins interact with B56α during adipocyte development. To address this, we transfected a FLAG-tagged B56α construct into differentiating 3T3-L1 cells at day 6 when B56α protein was observed to be maximally expressed (Fig 1). On day 6, we collected lysates, immunoprecipitated FLAG containing protein complexes, and identified associated peptides via mass spectrometry (Fig 3A). Along with the PP2A-A and -C subunits, we found prominent members of the β-catenin destruction complex. Specifically, proteins, Axin1, GSK3β, and Dvl1 were found to associate with FLAG-B56α at day 6 (Fig 3B). We confirmed interactions with Axin1 and GSK3β via immunoprecipitation in both 3T3-L1 and EMSCs (Fig 3C and D). We were not able to confirm Dvl1 in these complexes via immunoprecipitation, however that does not preclude its involvement in this process. Likely, Dvl1's role in the complex is associative and less likely to be direct. Interestingly, we found the interaction of B56α with the β-catenin destruction complex dramatically increased upon differentiation (Fig 3C and D). Next, we looked closer at the biochemistry involved with B56α and individual members of the β-catenin destruction complex identified in the proteomics screen. Using recombinant proteins to investigate binding *in vitro*, we found B56α preferably binds to GSK3β (Fig 3E). Next, we further defined the biochemical basis that mediates the interaction between B56α and GSK3β. Specifically, it has been reported that B56α subunit binds to a consensus short linear sequence on interacting proteins, termed the LxxI/VxE motif (Hertz *et al*, 2016).

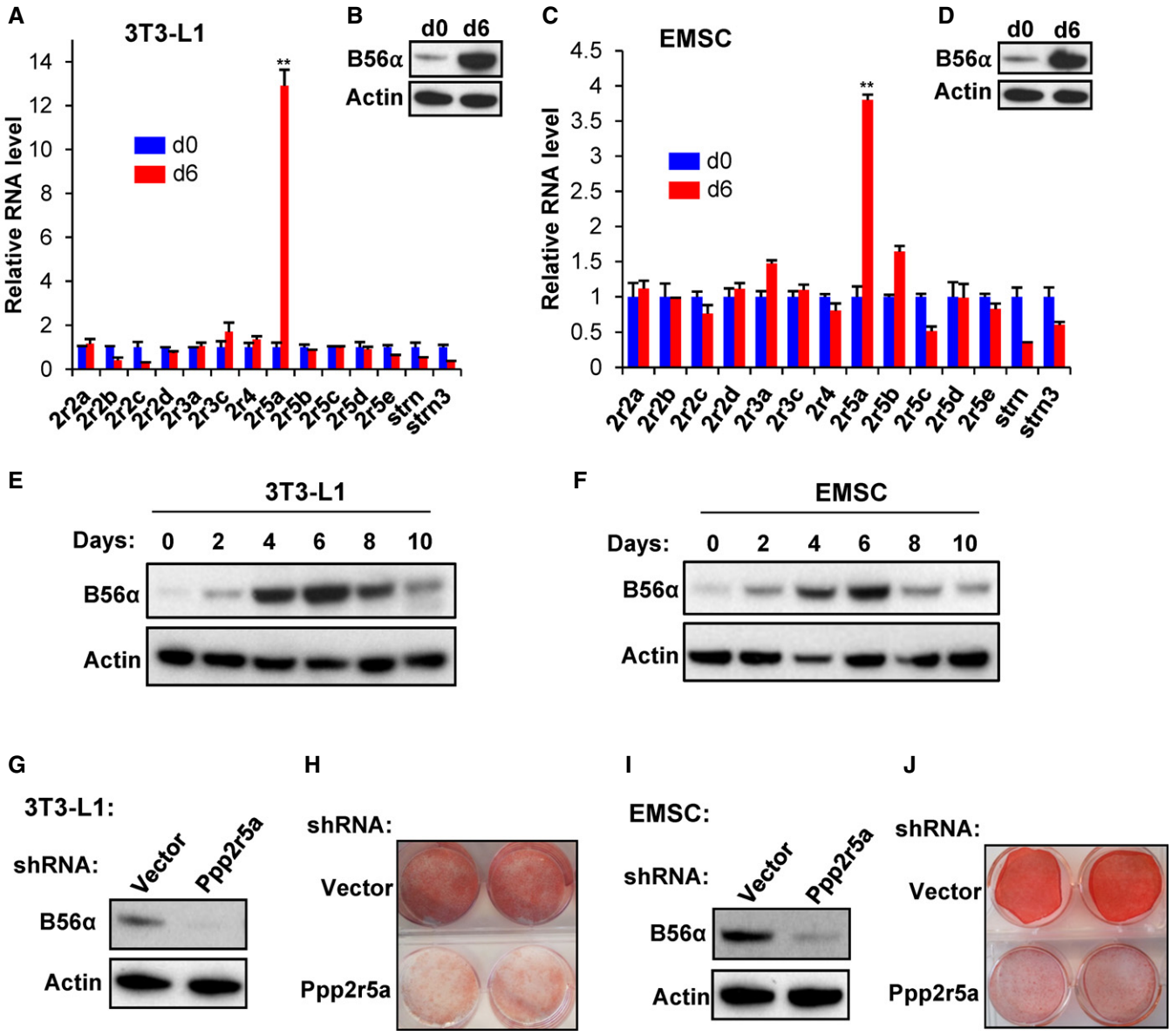

Figure 1. The PP2A-B subunit B56α is necessary for adipocyte differentiation.

A mRNA levels of indicated PP2A-B subunits at day 0 (blue) and day 6 (red) after induction of adipocyte differentiation in 3T3-L1 mouse pre-adipocytes.
B Western blot of B56α protein expression in 3T3-L1 cells at day 0 and day 6 after induction.
C mRNA levels of indicated PP2A-B subunits at day 0 (blue) and day 6 (red) after induction of adipocyte differentiation in mouse ear mesenchymal stem cells (EMSC).
D Western blot of B56α protein expression in EMSC at day 0 and day 6 after induction.
E Western blot of B56α expression at days indicated after induction in 3T3-L1 cells.
F Western blot of B56α expression at days indicated after induction in EMSCs.
G Western blot of B56α expression in empty vector or *Ppp2r5a* lentiviral shRNA-transduced 3T3-L1 cells at day 6 after induction.
H Oil Red O staining of empty vector or *Ppp2r5a* shRNA-transduced 3T3-L1 cells at day 10 following adipogenesis induction.
I Western blot of B56α expression in empty vector or *Ppp2r5a* shRNA-transduced EMSC at day 6 after induction.
J Oil Red O staining of empty vector or *Ppp2r5a* shRNA-transduced EMSC at day 10 following adipogenesis induction. $^{**}P < 0.01$ as measured by paired Student's *t*-test. Shown are representative data from experiments performed at least three times.

Source data are available online for this figure.

Interestingly, we found that GSK3β contains a conserved LxxI/VxE motif (Fig 3F). This consensus sequence is dependent upon aspartate at position 6. Thus, we mutated E137 of GSK3β to glutamate (E137D) to minimally disturb structural integrity and found the E137D mutant showed significantly decreased binding to B56α, whereas binding to Axin was diminished but still functional (Fig 3G), suggesting LxxI/VxE motif on GSK3β is critical for the interaction between GSK3β and B56α.

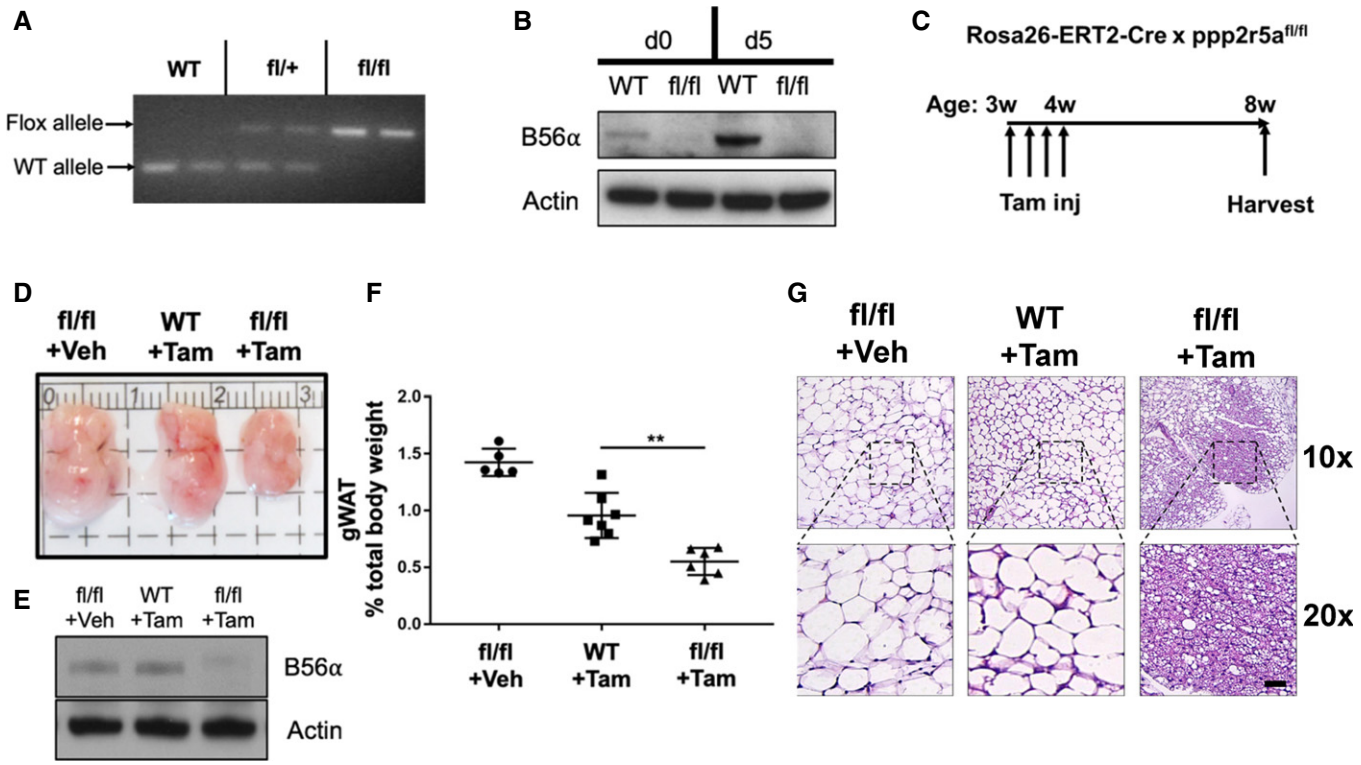

Figure 2. *Ppp2r5a* is necessary for gonadal white adipose development *in vivo*.

A Genotyping for the floxed allele of the *Ppp2r5a* gene taken F1 mice.
B Primary EMSCs isolated from WT and fl/fl mice were transduced with LV-Cre lentivirus and cultured in adipogenic induction medium for indicated days. Western blots showing loss of the B56α protein.
C Timeline and experimental strategy for gWAT development assay.
D Representative gWAT depots from WT and *Ppp2r5a fl/fl* mice.
E Western blot from gWAT tissue indicating loss of B56α expression.
F gWAT mass at 8 weeks. $^{**}P < 0.01$ as measured by unpaired Student's *t*-test.
G Hematoxylin and eosin staining for gWAT from indicated mice at 10× and 20× magnification. Scale bar equal to 20 microns.

Source data are available online for this figure.

The phosphorylation of GSK3β is dependent upon the expression of B56α

GSK3β phosphorylates β-catenin initiating its destruction and repressing its transcriptional activation. Downstream of Wnt ligand engagement however, one way Wnt activity is regulated is through GSK3β inhibition. GSK3β is phosphorylated at serine 9 and inactivated allowing β-catenin to accumulate and drive transcription (van Noort *et al*, 2002). In the context of adipocyte development, sustained Wnt signaling or β-catenin activation pushes pre-adipocytes toward osteoblast differentiation and away from adipocytes (Kang *et al*, 2007; Zeve *et al*, 2012). Since the phosphorylation status of GSK3β could affect relay of Wnt signaling, we monitored GSK3β phosphorylation at serine 9 throughout adipocyte

Figure 3. B56α protein–protein interactions during adipocyte development.

A 3T3-L1 cells were transduced with FLAG-*Ppp2r5a* retrovirus and induced toward adipogenesis. At day 6, after adipogenesis induction, protein was collected and immunoprecipitation was performed. Shown is a silver stain of the precipitates.
B List of highly enriched peptide IDs co-precipitating with FLAG-B56α as identified via mass spectrometry. Arrows indicate members of the PP2A phosphatase and β-catenin destruction complex.
C Immunoprecipitation and Western blot of FLAG-B56α transfected 3T3-L1 cells at day 6 after induction.
D Immunoprecipitation and Western blot of EMSCs. Representatives of at least three independent experiments are shown.
E GST pulldown and resulting Western blot (left) and silver stain (right).
F Schematic of GSK3β consensus sequence and proposed mechanism of PP2A/B/C de-phosphorylation.
G Western blot of 293T co-expression and immunoprecipitation with GSK3β point mutation E147D.

Source data are available online for this figure.

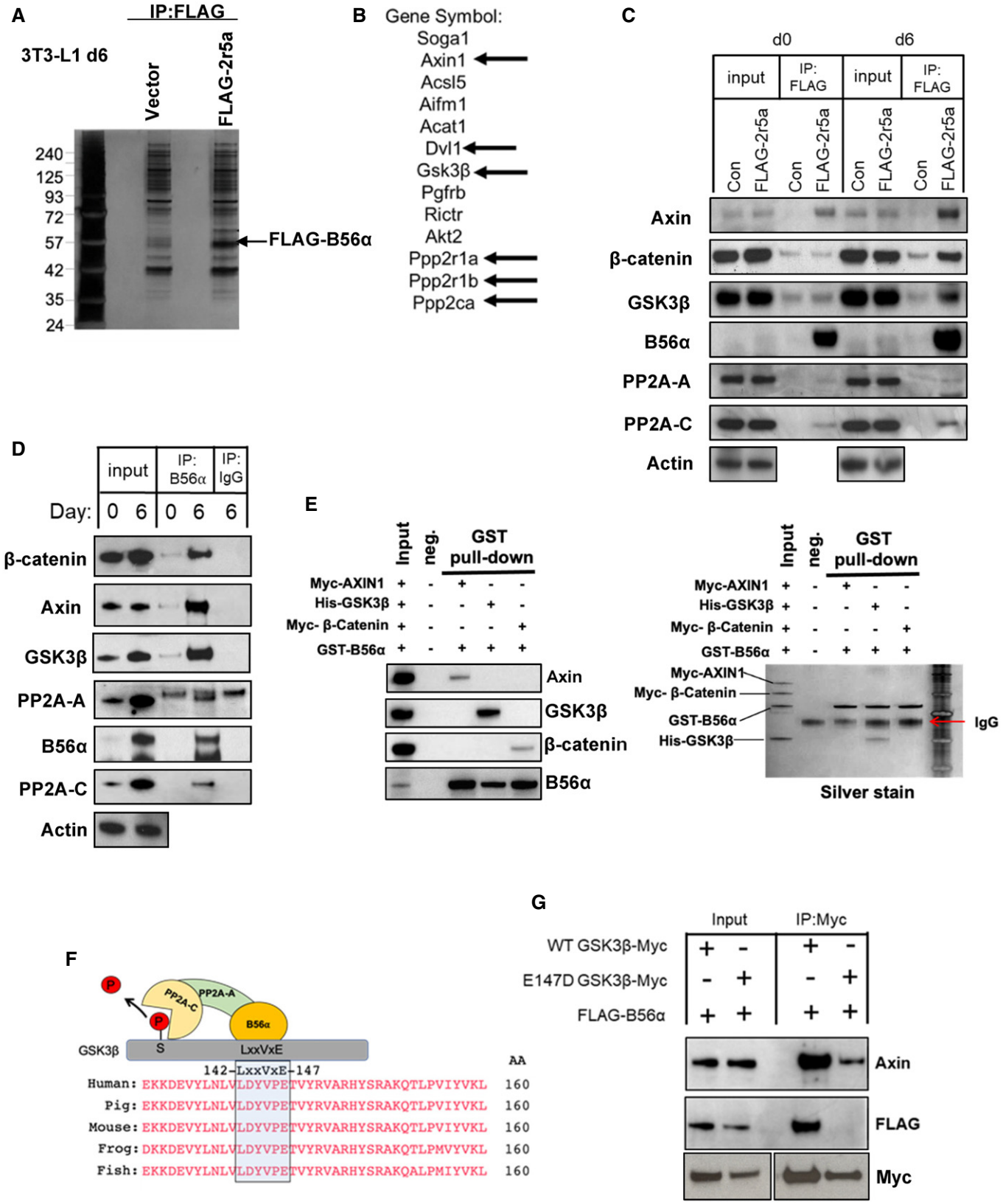
A
IP:FLAG
3T3-L1 d6
Vector
FLAG-2r5a
240
125
93
72
57
42
35
24
FLAG-B56α
B
Gene Symbol:
Soga1
Axin1
Acsl5
Aifm1
Acat1
Dvl1
Gsk3β
Pgfrb
Rictr
Akt2
Ppp2r1a
Ppp2r1b
Ppp2ca
C
d0
d6
input
IP: FLAG
Con
FLAG-2r5a
Axin
β-catenin
GSK3β
B56α
PP2A-A
PP2A-C
Actin
D
input
IP: B56α
IP: IgG
Day: 0 6 0 6 6
β-catenin
Axin
GSK3β
PP2A-A
B56α
PP2A-C
Actin
E
Input
neg.
GST pull-down
Myc-AXIN1
His-GSK3β
Myc- β-Catenin
GST-B56α
Axin
GSK3β
β-catenin
B56α
Myc-AXIN1
Myc- β-Catenin
GST-B56α
His-GSK3β
IgG
Silver stain
F
P
PP2A-C
PP2A-A
B56α
GSK3β
S
LxxVxE
142-LxxVxE-147
AA
Human: EKKDEVYLNLVLDYVPETVYRVARHYSRAKQTLPVIYVKL 160
Pig: EKKDEVYLNLVLDYVPETVYRVARHYSRAKQTLPVIYVKL 160
Mouse: EKKDEVYLNLVLDYVPETVYRVARHYSRAKQTLPVIYVKL 160
Frog: DKKDEVYLNLVLDYVPETVYRVARHYSRAKQTLPMVYVKL 160
Fish: EKKDEVYLNLVLDYVPETVYRVARHYSRAKQALPMIYVKL 160
G
Input
IP:Myc
WT GSK3β-Myc
E147D GSK3β-Myc
FLAG-B56α
Axin
FLAG
Myc

Figure 3.

development *in vitro*. Phosphorylation at Ser9 decreases starting at day 2 and was maintained at low levels until day 6. We found this pattern of phosphorylation is inversely correlated with B56α expression (Fig 4A). The phosphatase relationship with B56α is specific to Ser9 as phosphorylation at Tyr216, a separate activation mark (Hughes *et al*, 1993), did not correlate with B56α protein levels. We further tested the relationship between B56α expression and ph-GSK3β Ser9 by modulating expression of the *Ppp2r5a* gene. In EMSCs treated with shRNA targeting *Ppp2r5a* mRNA, we found GSK3β phosphorylation at Ser9 was sustained throughout the differentiation timeline (Fig 4B). Conversely, we decreased GSK3β Ser9 phosphorylation in cells transfected with a plasmid directing overexpression of the *Ppp2r5a* gene in 3T3-L1 cells (Fig 4C). Next, we utilized the *Ppp2r5a* knock-out system to test the relationship between ph-GSK3β Ser9 and B56α in isolated EMSCs from *Ppp2r5a*$^{fl/fl}$ mice and WT mice. Following transfection with lentiviral-Cre, we induced adipocyte differentiation and found GSK3β phosphorylation was sustained throughout the differentiation window in *Ppp2r5a*$^{fl/fl}$ compared to wild type (Fig 4D). Further, the loss of B56α completely blocked these cells from differentiating into cells capable of storing lipid (Fig 4E). These results demonstrate B56α expression has a profound effect on the phosphorylation status of GSK3β during adipocyte development.

Loss of B56α leads to accumulation of β-catenin and expression of osteoblast markers

The phosphorylation of GSK3β inactivates the kinase which should, in turn, result in increased accumulation of β-catenin and activation of canonical Wnt signaling (Salic *et al*, 2000). In the context of pre-adipocyte differentiation, sustained Wnt signaling could push development toward osteoblasts. Therefore, we took a closer look at Wnt signaling in the absence of *Ppp2r5a*. We first looked at the expression of both Wnt target genes and osteoblast differentiation genes in the absence of *Ppp2r5a* in EMSCs and found Wnt target genes *Axin2* (Yan *et al*, 2001) and *C-myc* (He *et al*, 1998) were significantly increased in the absence of *Ppp2r5a* at day 5 (Fig 5A). The osteoblast differentiation marker and Wnt target gene *Runx2* also increased significantly after differentiation (Gaur *et al*, 2005) indicating a potential push toward osteoblast differentiation in these cells. Moreover, we found increased expression of *Wnt10b*, an adipogenic inhibitor protein that has also been reported to increase upon GSK3β inhibition (Bennett *et al*, 2002). Our *in vivo* data suggest the gWAT is the primary organ affected by the loss of *Ppp2r5a*. To address this biology directly from the tissue, we harvested the stromal vascular fraction taken from adolescent fat pads of WT and *Ppp2r5a*$^{fl/fl}$ mice and induced adipocyte differentiation. We found these cells behaved similarly to EMSCs (Fig EV3A), suggesting the biological pathways found in 3T3-L1 and EMSCs are functional in gWAT. We next asked whether loss of B56α could produce sustained Wnt signaling and inhibit adipocyte differentiation markers *in vivo*. In RNA isolated from gonadal WAT, we found significant increases in the Wnt and osteoblast markers *Runx2, Pref1,* and *Wnt10b*, and a coordinate decrease in the adipose differentiation markers *Fabp4 and Plin1* (Fig 5B). We next used EMSCs derived from WT or *Ppp2r5a*$^{fl/fl}$ mice to look for activation of the Wnt pathway using the TCF/LEF reporter TOPFlash. We found that the luciferase reporter activity of *Ppp2r5a*$^{fl/fl}$ EMSCs was significantly higher than in the wild type in the absence of adipogenic stimuli. These data suggest increased activation of Wnt signaling in the absence of *Ppp2r5a* (Fig 5C). In mice knocked out for *Ppp2r5a*, we observed a dramatic increase in cell density, particularly near the edges of the tissue (Fig 2G). We used immunohistochemistry to stain for the presence of β-catenin in the gWAT collected from *Ppp2r5a* knock-out mice and compared the staining to wild-type samples. We found evidence of increased β-catenin staining in gWAT collected from these mice, particularly in areas of dense cellularity, which tended to be focused at the edge of the tissue (Fig 5D). Mice that constitutively express β-catenin in progenitor cells produce highly cellular, osteoblast-like tissue in the adipose compartments, including the storage of calcium (Zeve *et al*, 2012). Using Alizarin Red staining, we investigated for evidence of calcium accumulation in gWAT collected from *Ppp2r5a* knock-out mice. We found significant evidence of increased calcium in the adipose tissue, particularly near the dense cellular edges where β-catenin and active β-catenin staining was observed (Figs 5E and EV3B). Taken together, these data suggest loss of *Ppp2r5a* leads to increased β-catenin expression and an osteoblast phenotype in adipocytes and adipose tissue.

Expression of the *Ppp2r5a* gene is driven by PPARγ

Ppp2r5a mRNA expression is tightly controlled and transient (Fig 1). Taken together with its importance in modulating the Wnt signaling pathway and ultimately adipogenesis, we became interested in transcriptional regulation mechanisms for the *Ppp2r5a* gene. Using unbiased transcription factor consensus sequence scanning (Khan *et al*, 2018), we found a sequence 1,500 base pairs upstream of the *Ppp2r5a* gene with a highly aligned PPARγ response element or PPRE (Fig 6A). We found that supplementing adipogenic induction with troglitazone, a PPARγ agonist, for 24 h caused a significant increase in *Ppp2r5a* mRNA expression (Fig 6B). Moreover, we looked at previous studies that had performed ChIP-Seq

Figure 4. The phosphorylation of GSK3B is dependent upon the expression of B56α.

A Western blots from 3T3-L1 cells and EMSCs over time after adipocyte induction.

B Control or *Ppp2r5a* lentiviral shRNA-transduced EMSCs were used for adipocyte induction. Cell lysates were collected for Western blots at day 0 and day 6 after induction.

C Western blot using cell lysates from B56α-FLAG overexpression retrovirus infected 3T3-L1 cells.

D Western blots from EMSCs isolated from wild-type and *Ppp2r5a fl/fl* mice. Cells were transduced with LV-Cre lentivirus and cultured in adipogenic induction medium for indicated days.

E Oil Red O staining of EMSCs isolated from wild-type and *Ppp2r5a fl/fl* mice. Cells were transduced with LV-Cre lentivirus and cultured in adipogenic induction medium for 10 days.

Source data are available online for this figure.

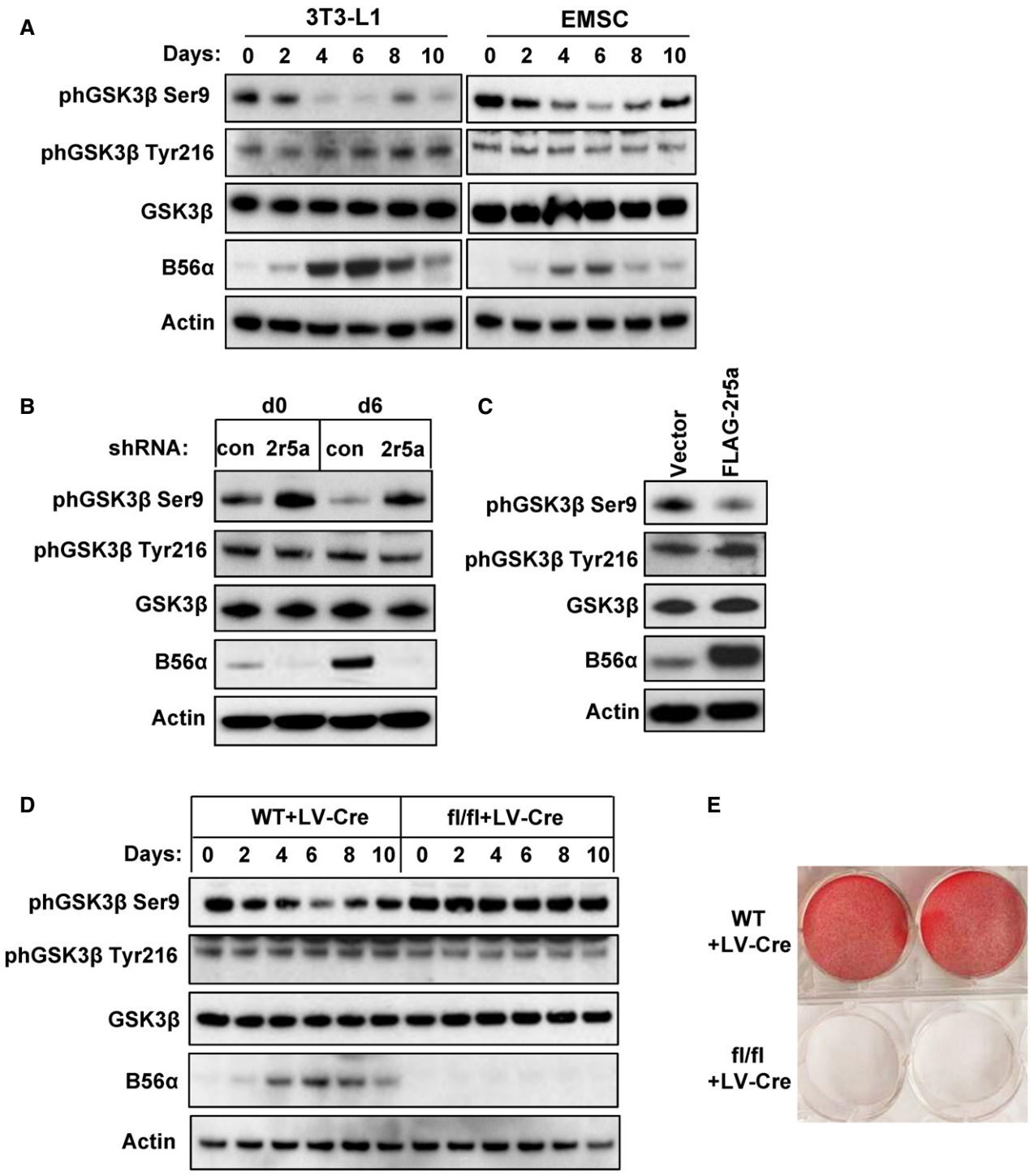

Figure 4.

experiments targeting either PPARγ or its transcriptional binding partner RXR (Haakonsson *et al*, 2013; Khan *et al*, 2018). Mapping the enriched reads to the genome revealed both PPARγ and RXR are enriched at the *Ppp2r5a* promoter surrounding the predicted consensus sequence during adipogenesis and in response to PPARγ agonist (Fig EV4A). To test this in our system, we designed three different probes that spanned the medial and distal regions of the *Ppp2r5a* promoter (Fig 6C). Using chromatin immunoprecipitation, we targeted PPARγ and investigated the enrichment. We found PPARγ occupied the *Ppp2r5a* promoter, specifically at the distal region where the consensus sequence is located (Fig 6D). Temporally, the occupation of PPARγ at the *Ppp2r5a* promoter correlates with the expression of the B56α protein observed in Fig 1. Moreover, the timeframe of *Ppp2r5a* promoter occupation by PPARγ aligns with

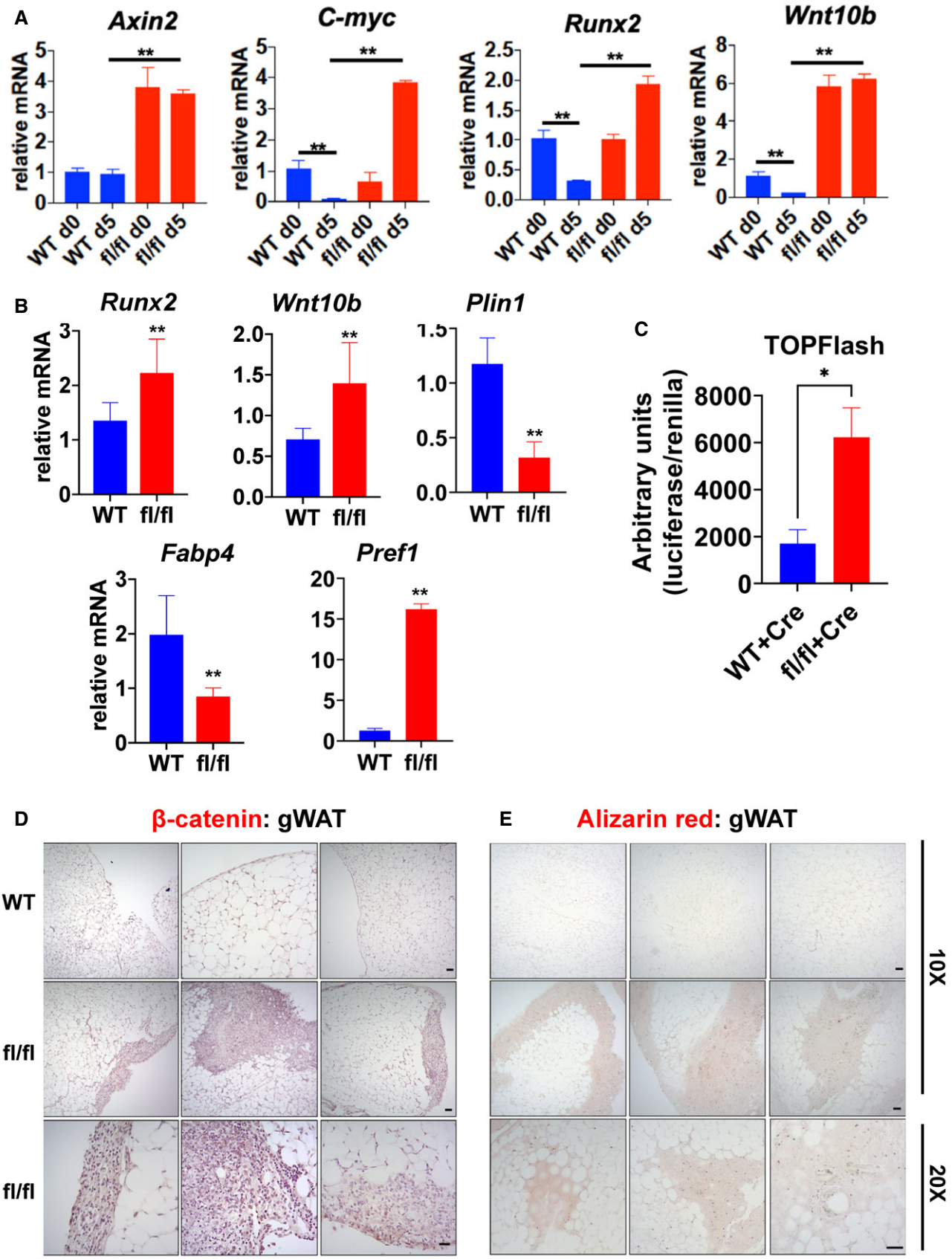

Figure 5.

Figure 5. Loss of B56α leads to accumulation of β-catenin and expression of osteoblast markers.

A mRNA expression of indicated genes from EMSCs treated with LV-Cre. $^{**}P < 0.01$ as measured by one way ANOVA. Shown are representatives of three independent experiments.

B mRNA expression of indicated genes from RNA isolated from the gWAT adipose tissue of mice at 8 weeks of age, 4 weeks after tamoxifen. $^{**}P < 0.01$ as measured by unpaired Student's *t*-test. $n = 6$ mice each group.

C TOPFlash reporter assay in unstimulated EMSCs $^{*}P < 0.01$ as measured by unpaired Student's *t*-test.

D Immunohistochemistry using an antibody targeting β-catenin in gWAT.

E Histology staining of gWAT using Alizarin Red to indicate calcium. Scale bar equal to 20 microns.

Source data are available online for this figure.

the occupation of another adipogenic marker *Fabp4* (Fig 6E). Interestingly, occupation of the promoter begins by 24 h, suggesting *Ppp2r5a* is part of the immediate early response during adipogenesis. We next cloned the distal and medial segments of the *Ppp2r5a* promoter into luciferase expression reporter constructs. Following the induction of 3T3-L1 cells, these constructs were transfected and monitored for response to troglitazone treatment. We found the distal promoter of *Ppp2r5a* to be troglitazone responsive demonstrating B56α expression is likely controlled by PPARγ (Fig 6F). Sustained activation of Wnt also blocks PPARγ signaling (Bennett *et al*, 2005), and when we looked at *Ppp2r5a* knock-out cells, we found significantly less expression of canonical PPARγ target genes in response to the PPARγ agonist troglitazone (Fig 6G). We next looked at the ability of troglitazone to induce adipogenesis in *Ppp2r5a* knock-out cells. Following infection with ADV-Cre-RFP, EMSCs were induced to differentiation with or without troglitazone. We found PPARγ activation with troglitazone could not rescue adipogenesis when *Ppp2r5a* was absent (Fig. EV4B–F). Taken together, these results demonstrate a relationship between PPARγ and adipogenesis through the expression and activity of *Ppp2r5a*.

PPARγ blockade of β-catenin activity is dependent on *Ppp2r5a*

The inverse relationship between PPARγ and canonical Wnt signaling represents an important crux of adipocyte development that remains without a direct mechanistic relationship. Therefore, we asked whether PPARγ control of β-catenin accumulation and Wnt signaling is through B56α. Primary EMSCs isolated from Rosa26 CRE ERT2 *Ppp2r5a*$^{fl/fl}$ and Rosa26 CRE ERT2 *Ppp2r5a*$^{wt/wt}$ were treated with 4-OHT overnight to induce Ppp2r5a knock-out and plated for induction. On day 3, upon the insulin maintenance stage of development, troglitazone or vehicle control was added along with insulin to stimulate PPARγ activation during adipogenesis. This is a well-established method to enhance adipocyte differentiation (Tafuri, 1996). We found that following 3 days of PPARγ activation, wild-type cells repress expression of active β-catenin in the cell measured by immunofluorescence targeting the active, un-phosphorylated (Ser3/37/Thr41) form (Fig 7A and B). Moreover, wild-type cells inhibit the expression of Wnt target genes throughout adipogenesis (Fig 7C) and form adipocytes capable of storing lipid (Fig 7D). However, in the absence of *Ppp2r5a*, β-catenin activation was sustained. Importantly, PPARγ activation by troglitazone was not able to decrease the expression of active β-catenin (Fig 7A and B) or Wnt target gene expression including the osteoblast differentiation factor *Runx2* (Fig 7C). In addition, administration of the PPARγ agonist troglitazone was not sufficient to rescue *Ppp2r5a* knock-out cells from differentiating into cells capable of storing lipid (Fig 7D). Taken together, these data demonstrate PPARγ control of the canonical Wnt signaling pathway is dependent on the expression of *Ppp2r5a*.

Discussion

As one of the major identified phosphatases, PP2A is expressed in a wide range of tissues and, as such, is implicated in disease and development. However, the ubiquitous nature of its expression makes it problematic to target therapeutically. Efforts to target the PP2A-A structural component or the PP2A-C catalytic subunit are likely to be stymied by widespread off-target effects in a variety of tissues. Here, we lay out a signaling axis during adipogenesis where a master transcription factor (PPARγ) drives the expression of a B subunit of the PP2A phosphatase (B56α) to influence the developmental fate of a cell. Moving forward, it will be interesting to connect other B subunits' selective expression and activity during critical signaling

Figure 6. *Ppp2r5a* is a PPARγ target gene.

A Alignment of the PPARγ consensus sequence and the −1,481 upstream sequence of *Ppp2r5a*.

B mRNA expression of the *Ppp2r5a* gene from EMSCs induced for 6 days and activated with troglitazone for 24 h. $^{**}P < 0.01$ as measured by paired Student's *t*-test. *Ppp2r5a* $^{fl/fl}$ and *Ppp2r5a* wild type are labeled as fl/fl and WT, respectively. Shown are representatives from three independent experiments.

C Schematic of the *Ppp2r5a* promoter and the medial (red, green) and distal (blue) regions probed for PPARγ binding.

D Chromatin immunoprecipitation targeting PPARγ and probing for medial and distal promoters of *Ppp2r5a*. Lysates were collected from day 6 EMSCs induced for adipogenesis. $^{**}P < 0.01$ as measured by one-way ANOVA. Shown are representatives from three independent experiments.

E FABP4 promoter ChIP from EMSCs induced for adipogenesis.

F The *Ppp2r5a* medial and distal promoter regions were cloned into luciferase reporter constructs, and luciferase reporter was measured in 3T3-L1 cells 5 days after induction ± troglitazone. $^{**}P < 0.01$ as measured by paired Student's *t*-test.

G mRNA expression of indicated genes from EMSCs transfected with LV-Cre and induced with troglitazone for 24 h. $^{**}P < 0.01$ as measured by unpaired Student's *t*-test. Shown are representatives from three independent experiments.

Source data are available online for this figure.

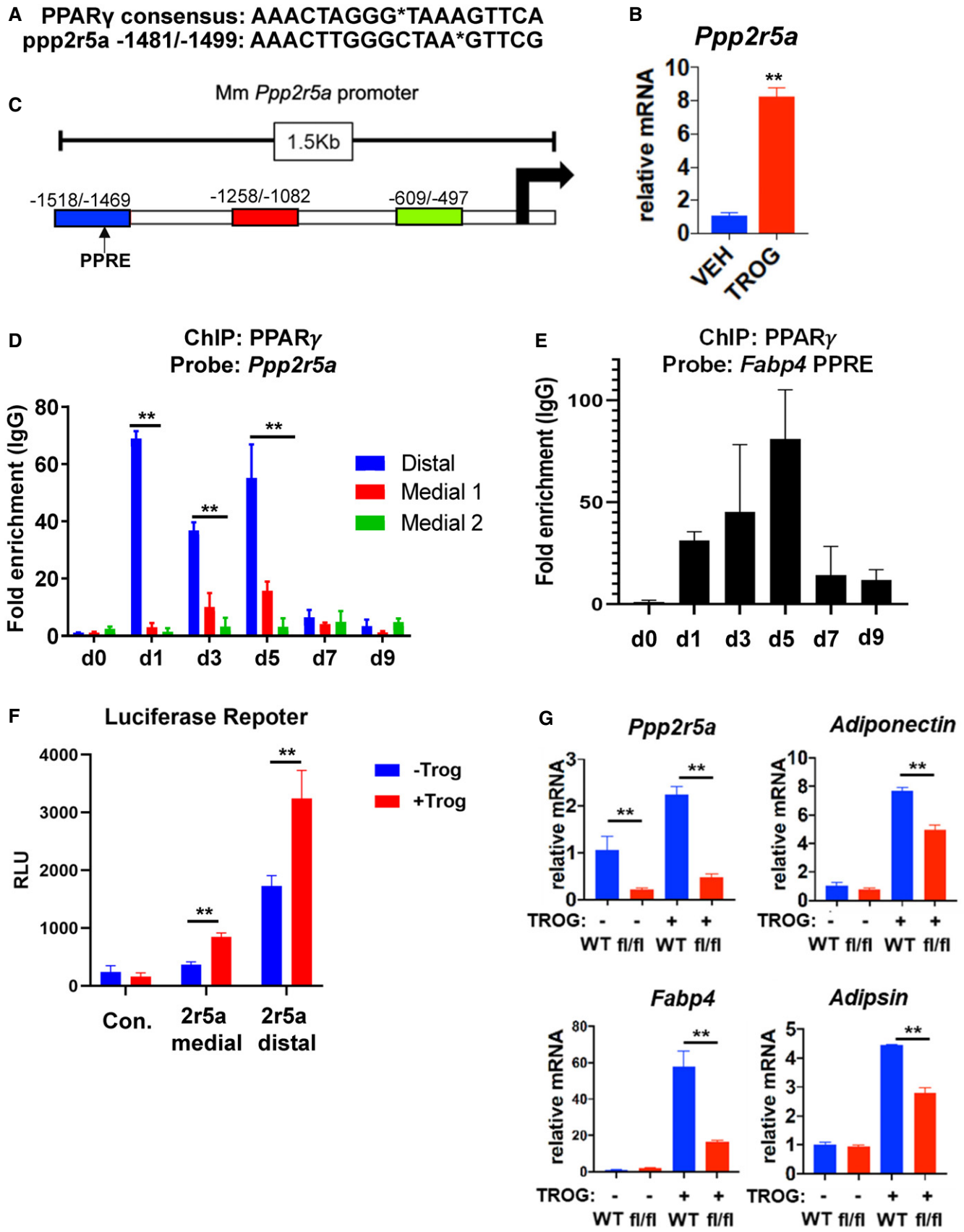

Figure 6.

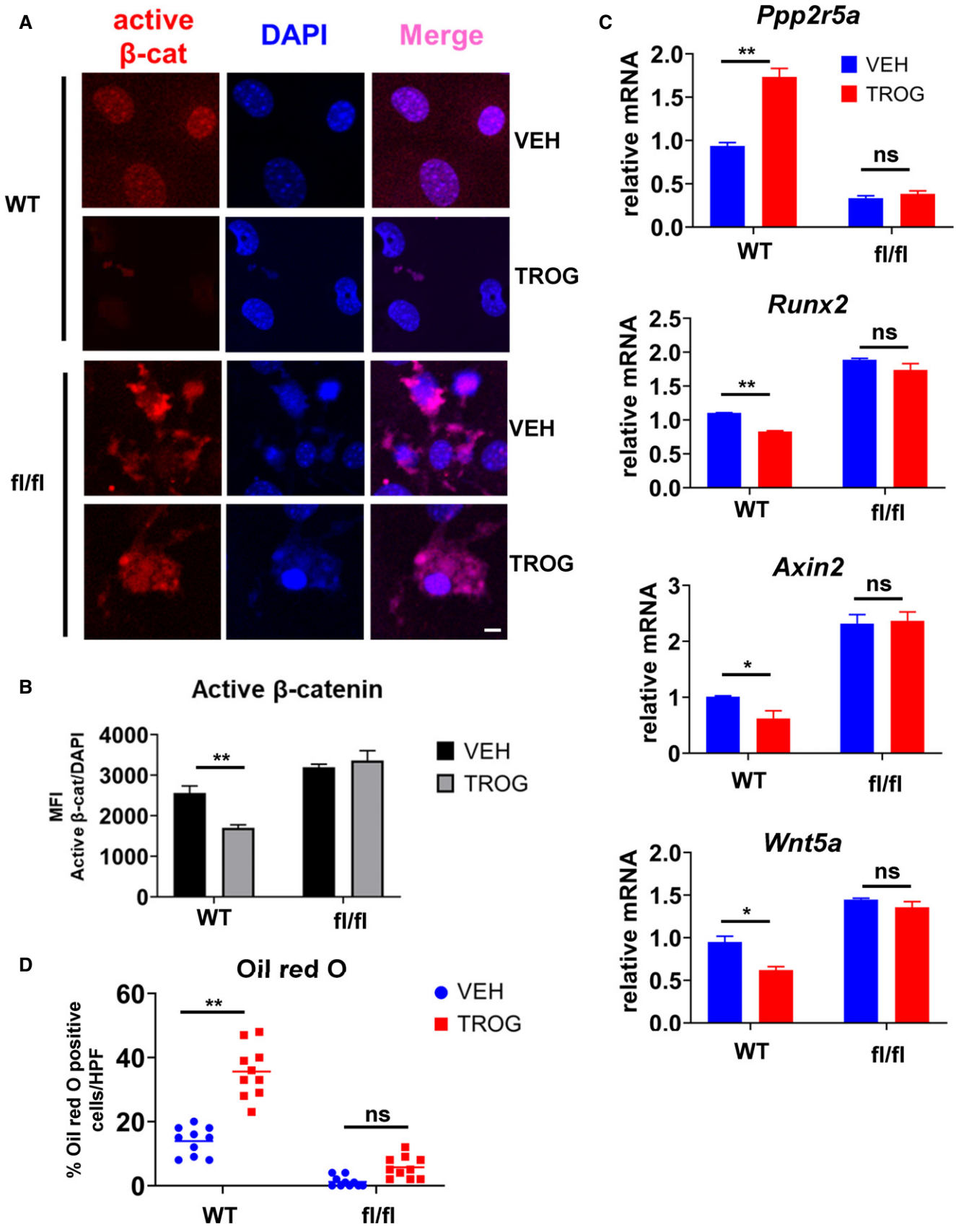
A
active β-cat
DAPI
Merge
WT
fl/fl
VEH
TROG
VEH
TROG
B
Active β-catenin
MFI Active β-cat/DAPI
4000
3000
2000
1000
0
**
VEH
TROG
WT
fl/fl
C
Ppp2r5a
relative mRNA
2.0
1.5
1.0
0.5
0.0
**
ns
VEH
TROG
WT
fl/fl
Runx2
relative mRNA
2.5
2.0
1.5
1.0
0.5
0.0
**
ns
WT
fl/fl
Axin2
relative mRNA
3
2
1
0
*
ns
WT
fl/fl
Wnt5a
relative mRNA
2.0
1.5
1.0
0.5
0.0
*
ns
WT
fl/fl
D
Oil red O
% Oil red O positive cells/HPF
60
40
20
0
**
ns
VEH
TROG
WT
fl/fl

Figure 7.

Figure 7. PPARγ blockade of β-catenin activity is dependent on B56α.

A Immunofluorescence for active-β-catenin (non-phospho Ser33/37/Thr41) in red and DAPI in blue. Expression was measured in EMSCs isolated from Rosa26 Cre WT and Rosa26 Cre *Ppp2r5a fl/fl*, treated with tamoxifen for 48 h, and induced toward adipogenesis. At day 3, troglitazone or vehicle was administered until day 10. Scale bar equal to 10 microns.

B Active β-catenin mean immunofluorescence intensity normalized to nuclei (DAPI). Shown is the average of ten 10× fields. $^{**}P < 0.01$ as measured by paired Student's *t*-test.

C mRNA expression of indicated genes from EMSCs induced toward adipogenesis at day 10. $^{*}P < 0.05$ and $^{**}P < 0.01$ as measured by paired Student's *t*-test. Shown are representative samples from 3 independent experiments.

D Percent Oil Red O^{+} cells per high-power field (10×). $^{**}P < 0.01$ as measured by paired Student's *t*-test.

Source data are available online for this figure.

cascades. The model outlined here could be a template for other processes that depend on phosphorylation as currency.

Corroborating our findings is an older study that identified a role for B56α in regulating Wnt signaling in Xenopus eggs (Li *et al*, 2001). Since then, much has been learned about this critical signaling pathway, yet the mechanism connecting the PP2A to Wnt has been elusive. The findings by Li and colleagues also implicate this mechanism in a broader tissue sense and suggest the biochemistry demonstrated in this study may apply to more tissue development and maintenance processes. Moreover, in the brain, a relationship between GSK3β, β-catenin, and the Ppp2r5d B subunit has been established (Louis *et al*, 2011). Our work adds significant mechanistic details to connect the PP2A phosphatase to the Wnt signaling pathway and opens the door to exploring this mechanism in other tissues and with different B subunits.

Canonical Wnt signaling is a highly conserved developmental pathway that centers around the accumulation of the transcription factor β-catenin which enters the nucleus to activate the expression of a network of genes implicated in fate differentiation, stemness, and cancer. β-catenin is destabilized in large part via glycogen synthase kinase 3β (GSK3β) phosphorylation (Yost *et al*, 1996). As a critical post-translational regulator of β-catenin levels, GSK3β has been and remains an interesting therapeutic target. GSK3β kinase activity itself is also controlled by upstream phosphorylation, primarily at serine 9 which renders it inactive (Frame *et al*, 2001). The mechanisms controlling Wnt shut down during adipogenesis have been looked at exhaustively and some conflicting data have emerged suggesting GSK3β phosphorylation may not be required for Wnt regulation (McManus *et al*, 2005; Taelman *et al*, 2010). Our data show B56α expression affects GSK3β S9 phosphorylation during adipocyte development, yet whether B56α modulates Wnt signaling via de-phosphorylating and activating GSK3β needs to be further explored. Our data suggest, at minimum, that B56α associates with β-catenin destruction complex and controls Wnt signaling.

In preliminary studies, we observed that whole-body knock-out induction either during embryogenesis or after birth resulted in gross developmental disruption and lethality, indicating *Ppp2r5a* plays a critical role in development. It is interesting to note other mouse models with suppressed *Ppp2r5a* expression either by hypomorphic expression (Janghorban *et al*, 2017) or by targeted disruption (Puhl *et al*, 2019) displayed an arrest in cellular differentiation or impact on cardiac responses to β-AR stimulation, suggesting an important role for B56α in physiological functions. Together, these data suggest *Ppp2r5a* is an essential gene and a minimal level of B56α expression is required for survival.

The PPARγ transcription factor also facilitates a critical pathway during adipogenesis (Rosen *et al*, 1999). Early during the pre-adipocyte to adipocyte transition, activation of PPARγ is required to drive the expression of the genes that equip the cells for lipid storage and define the mature adipocyte (Lefterova *et al*, 2008). Coordination of mechanisms, like those described here, between PPARγ and Wnt remains an interesting focus of attention in the adipose development field and beyond. The inverse relationship between PPARγ and Wnt has been known about for some time (Liu *et al*, 2006; Takada *et al*, 2009; Lecarpentier *et al*, 2017; Xie *et al*, 2018). In addition, although much has been done to understand PPARγ as a master adipogenic transcriptional regulator, evidence linking the biochemical relationships between PPARγ and Wnt remain mostly unknown. Our work highlights a novel mechanism connecting the two pathways during adipocyte development. Further studies looking at this relationship in other tissues will be of significant interest as aberrant expression of the Wnt signaling pathway is central to several cancer sub-types (Zhan *et al*, 2017). Glitazones have been prescribed as a first-line defense to diabetes to help re-sensitize tissues to insulin and are proficient in doing so (Fujita *et al*, 1983). However, some of the unintended side effects like increased adiposity in the bone marrow and loss of bone density (Stumvoll & Haring, 2002; Rzonca *et al*, 2004) have driven therapies away from glitazones. The mechanism described here provides a range of targets for therapeutic intervention focused on rebalancing the benefits PPARγ agonists have on diabetic patients. Our results suggest sustained PPARγ activity and thus B56α expression may deny the generation of new osteoblasts, as such intervention with B56α may provide new avenues to stabilize bone density in patients treated with PPARγ agonists.

Materials and Methods

Cell culture

3T3-L1 cells were acquired from the American Type Culture Collection and maintained in DMEM supplemented with 10% fetal bovine serum. For experiments, cells were plated to 70–80% confluency. To induce differentiation, at day 0 medium was replaced with adipose induction medium I (DMEM, insulin 5 μg/ml, dexamethasone 1 μM, IBMX 250 μM) for 48 h. Media was then replaced with adipose induction medium II (DMEM, insulin 5 μg/ml) for the remainder of the experiment. Media was replaced every 48 h.

Ear mesenchymal stem cells

Outer ear tissue was collected from 4- to 6-week-old C57/B6 mice into ice-cold PBS containing the anti-fungal Primocin. Tissue was

minced and incubated for 1 h at 37°C in Hank's balanced salt solution containing 2 mg/ml Collagenase type II (Worthington) and Primocin. Digested tissue was then passed through a 70-μM cell strainer, washed 1×, and plated in EMSC growth medium (DMEM, +10%FBS, +pen/strep). Cells were expanded through passage 5–7 times. For differentiation experiments, cells were plated at 250,000 cells/ml. To induce differentiation, at day 0 medium was replaced with adipose induction medium I (DMEM, insulin 5 μg/ml, dexamethasone 1 μM, IBMX 250 μM) for 48 h. Media was then replaced with adipose induction medium II (DMEM, insulin 5 μg/ml) for the remainder of the experiment. Media was replaced every 48 h.

Quantitative real-time PCR

RNA was collected in TRIzol (Invitrogen) and isolated according to the manufacturer's instructions. 500 ng or 1 μg of RNA was reverse-transcribed to cDNA using qScript (Quanta Bioscience). qPCRs were carried out using Perfecta SYBR Green (Quanta Bioscience) and analyzed on the Bio-Rad CFX machine (Bio-Rad). Thermal cycling was carried out as follows: 95°C for 10 s, 57.5°C for 30 s, and 65°C for 10 s, followed by a melt curve analysis to verify specificity. Data were analyzed using the delta delta Ct method. All samples were run in triplicate and normalized to an internal control. A complete list of primers can be found in Table EV1.

Western Blot

Cells were lysed in radioimmunoprecipitation assay buffer (RIPA) consisting of 150 mM NaCl, 25 mM Tris–HCl pH 7.4, NP-40 1%, sodium deoxycholate 0.5%, and SDS 0.1%. Prior to use, the cOmplete Protease/Phosphatase Inhibitor (Roche) was supplemented with RIPA. Protein lysates were chilled on ice for 10 min and centrifuged for 10 min at 4°C at 13,000 RPM. The supernatant was collected and subjected to the BCA assay to quantify protein. Protein samples were diluted in Laemmli buffer and boiled for 5 min at 95°C. 10–50 μg of protein was loaded and separated via SDS–PAGE on a 4–12% acrylamide gels for 1–2 h at 35 mA per gel. Protein was transferred to nitrocellulose at 150V for 1 h in the cold. Membranes were blocked for 1 h in 5% non-fat dry milk diluted in PBS + 0.5% Tween-20 (PBS-T). Membranes were washed 3 × 5 min with PBS-T. Primary antibodies were diluted in 2.5% bovine serum albumin diluted in PBS-T and incubated with membranes overnight at 4°C with rocking. Primary antibody was washed three times in PBS-T. Horseradish peroxidase-linked secondary antibody was added in 5% non-fat dry milk dissolved in PBS-T and incubated for 1hr at RT with rocking. Membranes were washed 3X in PBS-T for 10 min each. For imaging, membranes were incubated for 5 min in Western Lighting Plus ECL (PerkinElmer) reagent. Membranes were exposed to Hyperfilm (GE Healthcare). A complete list of antibodies used can be found in Table EV2.

Generation of *Ppp2r5a* floxed mice

Targeted iTL IC1, C57BL/6 embryonic stem cells were microinjected into BALB/C blastocysts. Resulting chimeras with a high percentage black coat color were mated to C57BL/6 FLP mice to remove the Neo cassette. Tail DNA was analyzed as described below from pups with black coat color. Primer set NDEL1 and NDEL2 was used to screen mice for the deletion of the Neo cassette. The PCR product for the wild type is 157 bp. After Neo deletion, one set of LoxP-FRT sites remain PCR was performed to detect presence of the distal LoxP site. All genotyping primers are available in Table EV1. Mice were bred to homozygosity and used for experiments and further breeding as described below.

Mouse experiments

All mouse experiments were carried out in accordance with and under the supervision of the University of California Irvine and City of Hope Beckman Research Center Institutional Animal Care and Use Committees. The Rosa26 Cre-ERT2 mouse was obtained from Jackson Laboratories and bred to the Ppp2r5a fl/fl mice until heterozygous for Rosa26 Cre-ERT2 and homozygous for Ppp2r5a floxed. Mice were genotyped via tail snip using the primers provided by Jackson Laboratories for Rosa26 Cre-ERT2 and primers we designed which probe the interface between the recombination event and the wild-type gene. At day 21, mice were sexed and weaned and injected with 100 μl of 10 mg/ml tamoxifen dissolved in corn oil intraperitoneally four times over the course of 1 week. Mice were fed standard chow ad libitum and monitored daily for food intake and overt signs of distress. Mouse experiments were conducted using a mix of male and female mice.

Constructs

To generate mouse *Ppp2r5a* overexpression vector, mouse cDNA was used as PCR template to amplify *Ppp2r5a* cDNA sequence with primers 2r5a-cF: 5′ (BamH I) G**GGATCC**ATGGACTACAAGGACGACGATGACAAGTCGTCGCCGTCGCCGCCCGCAC, 2r5a-cR: 5′ (Xho I) G**CTCGAG**TTATTTGGCACTGGTACTGCTG (bold letters are restriction sites, underlined nucleotides is Flag tag). The PCR products were cloned into pCR2.1-TOPO vector and sequenced. Then, *Ppp2r5a* cDNA was cloned from pCR2.1-TOPO into pLPC-NFLAG vector by BamH I and Xho I enzymatic digestion. To generate wild-type pLPC-Gsk3b-Myc vector, full-length cDNA of mouse Gsk3b was purchased from Sino Biological, Inc (MG50650-CM). The cDNA sequence and Myc tag were then amplified by PCR with primers mGSK3b-cF: 5′-ATGTCGGGGCGACCGAGAACCAC-3′ and mGSK3b-cR: 5′-TTACAGATCCTCTTCTGAGATGAG-3′. The PCR products were cloned into pCR2.1-TOPO vector. The pLPC-NFLAG vector was digested with restriction enzymes Kpn I and Not I to remove Flag tag. Then, the Myc-tagged Gsk3b was cut from pCR2.1-TOPO by Kpn I and Not I enzymatic digestion and ligated to pLPC vector. For E137D pLPC-Gsk3b-Myc mutant vector generation, mutagenesis primers (mGSK3b E137D F2: 5′-TCCGGACACAGTGTACAGAGT-3′ and mGSK3b E137D R: 5′-AC ATAGTCCAGCACCAGGTTAAGG-3′) were used to amplify the vector pCR2.1-TOPO-Gsk3b-Myc by PCR. The mutant Gsk3b-Myc was then sequenced and moved from pCR2.1-TOPO to pLPC-NFLAG vector by Kpn I and Not I enzymatic digestion similar as wild-type Gsk3b-Myc.

Transfection and transduction

To generate retro viral particles for B56α or GSK3β overexpression, 293T cells in a 6-cm plate were co-transfected with 10 μg pLPC-

B56α or pLPC-GSK3β and 5 μg helper virus using Lipofectamine 2000. To generate lentiviral particles for shRNA knock-down, 293T cells in a 6-cm dish were co-transfected with 2.5 μg pLKO.1 empty vector or shRNA vector, 1.25 μg pMDL, 0.625 μg pCMV-VSV-G, and 0.625 μg pRSV-Rev (4:2:1:1). Viral supernatants were collected after 48 and 72 h. Cells were infected with the virus for two to four times throughout 48 h. Puromycin was added 2 days after infection to select positively infected cells. Plasmids containing TRC lentiviral shRNA of mouse Ppp2r5a (TRCN0000081185) were purchased from Dharmacon.

Immunohistochemistry

Tissue was collected in 37% formalin. Samples were processed into paraffin blocks, and slides were cut by the University of California Irvine histology core. For staining, de-paraffinization and rehydration was carried out as follows: incubations of 5 min each: xylene (three washes), 100% ethanol, 95% ethanol, and water (two washes). Slides were then boiled in Citrate Unmasking solution (Cell Signaling) and incubated for 10 min. Slides were then washed in water twice for 5 min. Slides were incubated in 3% hydrogen peroxide for 10 min and washed in water twice and then TBS-T twice. Samples were blocked in normal goat serum for 1 h at RT. Primary anti-B-catenin antibody (Cell Signaling) was diluted 1:100 and added overnight in a humidified chamber. Slides were washed three times with TBST. SignalStain Boost Detection Reagent anti-rabbit HRP (Cell Signaling) was added to samples and incubated for 1 h at RT. Slides were washed three times with TBS-T and incubated with NovaRed HRP activation agent as per the manufacturer's instructions (Vector). Slides were dipped in water and counterstained with hematoxylin for 30 s. Slides were washed in water until clear and dehydrated with 95% ethanol, 100% ethanol, and xylene twice for 10 s each. Slides were mounted with Permount (Fisher) and examined using the Seba3 RC-3 microscope (Laxco).

Oil Red O staining

Medium was removed from cells and washed with twice in PBS. 10% formalin was added to each well and incubated for 1 h at RT. Cells were washed twice with water. 60% isopropanol was added to each well for 5 min and then removed. Oil Red O working solution was added (1 mg/ml Oil Red O in isopropanol/water) for 20 min with rotation. Staining solution was removed, and wells were washed three times with water. Hematoxylin/eosin was added for 30 s and then washed three times with water. Cells were observed using the Evos Fluor inverted microscope.

Alizarin Red staining

Sections were de-paraffinized in xylene 2×, 100% ethanol 2×, 95% ethanol, 90% ethanol, 80% ethanol, and 70% ethanol each for 5 min. Slides were next washed in water briefly. Sections were then incubated in 200 mg/ml Alizarin Red solution (Sigma) for 5 min. Slides were shaken dry and dipped in acetone repeatedly, then acetone/xylene 1:1, and then xylene. Slides were mounted with Permount (Fisher). Slides were examined using the Seba3 RC-3 microscope (Laxco).

Immunoprecipitation

200–500 μg of RIPA lysates collected as indicated above (Western blot) were diluted to 500 μl, precleared with normal protein A or protein G agarose beads, and subjected to immunoprecipitation using 1 μg of specific antibody or corresponding species IgG control overnight at 4°C with rocking. Protein A or protein G agarose was added for 1 h, and beads were washed with 1 ml RIPA buffer 3× with 3,000RPM spins at 4°C in between washes. Beads were resuspended in Laemmli buffer and analyzed via Western blot.

In vitro binding assays

To examine the interaction between B56α and complex β-catenin/GSK3β/AXIN1, 2 μg of recombinant GST-B56α was mixed with equal amount of recombinant Myc-β-catenin, His-GSK3β, or Myc-AXIN1. A tube with all these four proteins was set as a control. The mixture was incubated at 37°C for 30 min in 200 μl of assay buffer (25 mM Tris [pH 8.0], 150 mM NaCl, 2 mM dithiothreitol, and 1 mg/ml). Glutathione Sepharose 4B resin was then added to the samples for GST-tag binding. The samples were washed for three times with assay buffer and examined by Western blot with indicated antibodies. GST-B56α was purchased from Abnova (H00005525-P01), His-GSK3β was purchased from Life Technologies (PV3365), and Myc-β-catenin and Myc-AXIN1 were purchased from OriGene (TP308349, TP308947).

Luciferase reporter assays

The TOPFlash (Tcf reporter) construct was obtained from Millipore (21–170) and transfected along with pRL renilla control (10:1) into EMSCs using Lipofectamine 2000 at day 3 after seeding. At day 5 after seeding, cells were harvested and monitored for luciferase and renilla luminescence using the Promega (E1910) dual luciferase reporter assay system. Luciferase was normalized to renilla expression. For the *Ppp2r5a* reporter, medial and distal regions of the P*pp2r5a* promoter were cloned upstream of the luciferase cassette in the pBV-luc construct. These constructs along with an empty vector control were transfected into 3T3-L1 cells at day 3 after induction of adipogenesis. At day 5, cells were harvested and luciferase was measured according to the manufacturers' protocol from the Promega dual luciferase assay as above. Luciferase was normalized to protein concentration.

Chromatin immunoprecipitation

Cross-linking was carried out in 1% formaldehyde added to culture medium containing 1–2E6 cells for 10 min. Cells were collected in cold PBS supplemented with cOmplete Protease Inhibitors (Roche) and gently pelleted. The supernatant was removed, and the pellet was resuspended in 500 μl SDS lysis buffer supplemented with protease inhibitors. Sonication was carried out at 4°C using the sonicator at 30% and five pulses of 20 s on 30 s off on ice. Sonicates were diluted fivefold in ChIP dilution buffer (Millipore) and precleared for 30 min with 30 μl Protein A agarose/salmon sperm DNA. At this point, 1% of the lysate was collected as input. The rest of the lysate was subjected to immunoprecipitation with 1 μg of anti-PPARγ antibody or 1 μg of anti-mouse IgG overnight at 4°C with rotation. Next, 10 μl of protein A ChIP grade magnetic beads

(Cell Signaling) were added for 1 h with rotation. Immunoprecipitates were washed with low salt, high salt, lithium chloride, and TE buffers. DNA/protein complexes were eluted from the antibody/beads in 1% SDS 0.1 M sodium bicarbonate for 15 min. To reverse the cross-links, 20 μl of 5 M NaCl was added and the samples were incubated at 65°C overnight. Samples were then treated with 10 μl 500 mM EDTA and 20 μl 1 M Tris–HCl pH 6.5 and proteinase K and incubated at 45°C for 1 h. Samples, including the input samples, were then purified through a PCR purification kit (Qiagen) and recovered in water. RT–PCR was performed on the samples using the primers found in Table EV1.

Statistical analysis

Data are shown as the mean ± standard error of the mean. Significance between samples was calculated using Student's *t*-test whether paired or unpaired dependent on the experiment and noted in the figure legends. Specific *P* values and sample information can be found in the figure legends.

Data availability

No data were deposited in a public database.

Expanded View for this article is available online.

Acknowledgements
We thank members of the Kong laboratory for helpful discussions. We also thank Raquel Chamorro-Garcia and the Bruce Blumberg laboratory for assistance with *in vivo* analysis. This work was supported by the American Cancer Society RSG-16-085-01-TBE (MK), PFDDC-132846 (EAH), and National Institute of Health 5T32CA009054 (EAH).

Author contributions
EAH, MP, YY, MBIG, TQT, WL, and XHL performed experiments and analyzed data. QAW evaluated experiments and analyzed data. MP performed *in vitro* experiments and protein binding experiments and developed the *Ppp2r5a fl/fl* mouse. BR contributed to manuscript preparation. EAH performed binding experiments, mouse experiments, and PPARγ experiments and wrote the manuscript. MK supervised the study.

Conflict of interest
The authors declare that they have no conflict of interest.

References

Bennett CN, Ross SE, Longo KA, Bajnok L, Hemati N, Johnson KW, Harrison SD, MacDougald OA (2002) Regulation of Wnt signaling during adipogenesis. *J Biol Chem* 277: 30998 – 31004

Bennett CN, Longo KA, Wright WS, Suva LJ, Lane TF, Hankenson KD, MacDougald OA (2005) Regulation of osteoblastogenesis and bone mass by Wnt10b. *Proc Natl Acad Sci USA* 102: 3324 – 3329

Berry DC, Stenesen D, Zeve D, Graff JM (2013) The developmental origins of adipose tissue. *Development* 140: 3939 – 3949

Collaboration NCDRF (2019) Rising rural body-mass index is the main driver of the global obesity epidemic in adults. *Nature* 569: 260 – 264

Eichhorn PJ, Creyghton MP, Bernards R (2009) Protein phosphatase 2A regulatory subunits and cancer. *Biochim Biophys Acta* 1795: 1 – 15

Frame S, Cohen P, Biondi RM (2001) A common phosphate binding site explains the unique substrate specificity of GSK3 and its inactivation by phosphorylation. *Mol Cell* 7: 1321 – 1327

Fujita T, Sugiyama Y, Taketomi S, Sohda T, Kawamatsu Y, Iwatsuka H, Suzuoki Z (1983) Reduction of insulin resistance in obese and/or diabetic animals by 5-[4-(1-methylcyclohexylmethoxy)benzyl]-thiazolidine-2,4-dione (ADD-3878, U-63,287, ciglitazone), a new antidiabetic agent. *Diabetes* 32: 804 – 810

Gaur T, Lengner CJ, Hovhannisyan H, Bhat RA, Bodine PVN, Komm BS, Javed A, van Wijnen AJ, Stein JL, Stein GS *et al* (2005) Canonical WNT signaling promotes osteogenesis by directly stimulating Runx2 gene expression. *J Biol Chem* 280: 33132 – 33140

Gotz J, Schild A (2003) Transgenic and knockout models of PP2A. *Methods Enzymol* 366: 390 – 403

Haakonsson AK, Stahl Madsen M, Nielsen R, Sandelin A, Mandrup S (2013) Acute genome-wide effects of rosiglitazone on PPARgamma transcriptional networks in adipocytes. *Mol Endocrinol* 27: 1536 – 1549

He TC, Sparks AB, Rago C, Hermeking H, Zawel L, da Costa LT, Morin PJ, Vogelstein B, Kinzler KW (1998) Identification of c-MYC as a target of the APC pathway. *Science* 281: 1509 – 1512

Hertz EPT, Kruse T, Davey NE, López-Méndez B, Sigurðsson JO, Montoya G, Olsen JV, Nilsson J (2016) A conserved motif provides binding specificity to the PP2A-B56 phosphatase. *Mol Cell* 63: 686 – 695

Hughes K, Nikolakaki E, Plyte SE, Totty NF, Woodgett JR (1993) Modulation of the glycogen synthase kinase-3 family by tyrosine phosphorylation. *EMBO J* 12: 803 – 808

Janghorban M, Langer EM, Wang X, Zachman D, Daniel CJ, Hooper J, Fleming WH, Agarwal A, Sears RC (2017) The tumor suppressor phosphatase PP2A-B56α regulates stemness and promotes the initiation of malignancies in a novel murine model. *PLoS One* 12: e0188910

Janssens V, Goris J (2001) Protein phosphatase 2A: a highly regulated family of serine/threonine phosphatases implicated in cell growth and signalling. *Biochem J* 353: 417 – 439

Kang S, Bennett CN, Gerin I, Rapp LA, Hankenson KD, Macdougald OA (2007) Wnt signaling stimulates osteoblastogenesis of mesenchymal precursors by suppressing CCAAT/enhancer-binding protein alpha and peroxisome proliferator-activated receptor gamma. *J Biol Chem* 282: 14515 – 14524

Khan A, Fornes O, Stigliani A, Gheorghe M, Castro-Mondragon JA, van der Lee R, Bessy A, Cheneby J, Kulkarni SR, Tan G *et al* (2018) JASPAR 2018: update of the open-access database of transcription factor binding profiles and its web framework. *Nucleic Acids Res* 46: D1284

Kusminski CM, Bickel PE, Scherer PE (2016) Targeting adipose tissue in the treatment of obesity-associated diabetes. *Nat Rev Drug Discov* 15: 639 – 660

Lecarpentier Y, Claes V, Vallee A, Hebert JL (2017) Interactions between PPAR gamma and the canonical Wnt/beta-catenin pathway in type 2 diabetes and colon cancer. *PPAR Res* 2017: 5879090

Lefterova MI, Zhang Y, Steger DJ, Schupp M, Schug J, Cristancho A, Feng D, Zhuo D, Stoeckert Jr CJ, Liu XS *et al* (2008) PPARgamma and C/EBP factors orchestrate adipocyte biology via adjacent binding on a genome-wide scale. *Genes Dev* 22: 2941 – 2952

Li X, Yost HJ, Virshup DM, Seeling JM (2001) Protein phosphatase 2A and its B56 regulatory subunit inhibit Wnt signaling in *Xenopus*. *EMBO J* 20: 4122 – 4131

Liu J, Wang H, Zuo Y, Farmer SR (2006) Functional interaction between peroxisome proliferator-activated receptor gamma and beta-catenin. *Mol Cell Biol* 26: 5827 – 5837

Louis JV, Martens E, Borghgraef P, Lambrecht C, Sents W, Longin S, Zwaenepoel K, Pijnenborg R, Landrieu I, Lippens G *et al* (2011) Mice lacking phosphatase PP2A subunit PR61/B'delta (Ppp2r5d) develop spatially restricted tauopathy by deregulation of CDK5 and GSK3beta. *Proc Natl Acad Sci USA* 108: 6957 – 6962

McManus EJ, Sakamoto K, Armit LJ, Ronaldson L, Shpiro N, Marquez R, Alessi DR (2005) Role that phosphorylation of GSK3 plays in insulin and Wnt signalling defined by knockin analysis. *EMBO J* 24: 1571 – 1583

van Noort M, Meeldijk J, van der Zee R, Destree O, Clevers H (2002) Wnt signaling controls the phosphorylation status of beta-catenin. *J Biol Chem* 277: 17901 – 17905

Puhl SL, Weeks KL, Güran A, Ranieri A, Boknik P, Kirchhefer U, Müller FU, Avkiran M (2019) Role of type 2A phosphatase regulatory subunit B56α in regulating cardiac responses to β-adrenergic stimulation *in vivo*. *Cardiovasc Res* 115: 519 – 529

Reid MA, Wang WI, Rosales KR, Welliver MX, Pan M, Kong M (2013) The B55alpha subunit of PP2A drives a p53-dependent metabolic adaptation to glutamine deprivation. *Mol Cell* 50: 200 – 211

Rim JS, Mynatt RL, Gawronska-Kozak B (2005) Mesenchymal stem cells from the outer ear: a novel adult stem cell model system for the study of adipogenesis. *FASEB J* 19: 1205 – 1207

Rosen ED, Sarraf P, Troy AE, Bradwin G, Moore K, Milstone DS, Spiegelman BM, Mortensen RM (1999) PPAR gamma is required for the differentiation of adipose tissue *in vivo* and *in vitro*. *Mol Cell* 4: 611 – 617

Rzonca SO, Suva LJ, Gaddy D, Montague DC, Lecka-Czernik B (2004) Bone is a target for the antidiabetic compound rosiglitazone. *Endocrinology* 145: 401 – 406

Salic A, Lee E, Mayer L, Kirschner MW (2000) Control of beta-catenin stability: reconstitution of the cytoplasmic steps of the wnt pathway in Xenopus egg extracts. *Mol Cell* 5: 523 – 532

Sangodkar J, Farrington CC, McClinch K, Galsky MD, Kastrinsky DB, Narla G (2016) All roads lead to PP2A: exploiting the therapeutic potential of this phosphatase. *FEBS J* 283: 1004 – 1024

Seshacharyulu P, Pandey P, Datta K, Batra SK (2013) Phosphatase: PP2A structural importance, regulation and its aberrant expression in cancer. *Cancer Lett* 335: 9 – 18

Shi Y (2009) Serine/threonine phosphatases: mechanism through structure. *Cell* 139: 468 – 484

Stumvoll M, Haring HU (2002) Glitazones: clinical effects and molecular mechanisms. *Ann Med* 34: 217 – 224

Taelman VF, Dobrowolski R, Plouhinec JL, Fuentealba LC, Vorwald PP, Gumper I, Sabatini DD, De Robertis EM (2010) Wnt signaling requires sequestration of glycogen synthase kinase 3 inside multivesicular endosomes. *Cell* 143: 1136 – 1148

Tafuri SR (1996) Troglitazone enhances differentiation, basal glucose uptake, and Glut1 protein levels in 3T3-L1 adipocytes. *Endocrinology* 137: 4706 – 4712

Takada I, Kouzmenko AP, Kato S (2009) Wnt and PPARgamma signaling in osteoblastogenesis and adipogenesis. *Nat Rev Rheumatol* 5: 442 – 447

Virshup DM, Shenolikar S (2009) From promiscuity to precision: protein phosphatases get a makeover. *Mol Cell* 33: 537 – 545

Xie Y-Y, Mo C-L, Cai Y-H, Wang W-J, Hong X-X, Zhang K-K, Liu Q-F, Liu Y-J, Hong J-J, He T *et al* (2018) Pygo2 regulates adiposity and glucose homeostasis via β-catenin-axin2-GSK3β signaling pathway. *Diabetes* 67: 2569 – 2584

Yan D, Wiesmann M, Rohan M, Chan V, Jefferson AB, Guo L, Sakamoto D, Caothien RH, Fuller JH, Reinhard C *et al* (2001) Elevated expression of axin2 and hnkd mRNA provides evidence that Wnt/beta -catenin signaling is activated in human colon tumors. *Proc Natl Acad Sci USA* 98: 14973 – 14978

Ye R, Wang QA, Tao C, Vishvanath L, Shao M, McDonald JG, Gupta RK, Scherer PE (2015) Impact of tamoxifen on adipocyte lineage tracing: inducer of adipogenesis and prolonged nuclear translocation of Cre recombinase. *Mol Metab* 4: 771 – 778

Yost C, Torres M, Miller JR, Huang E, Kimelman D, Moon RT (1996) The axis-inducing activity, stability, and subcellular distribution of beta-catenin is regulated in Xenopus embryos by glycogen synthase kinase 3. *Genes Dev* 10: 1443 – 1454

Zeve D, Seo J, Suh J, Stenesen D, Tang W, Berglund E, Wan Y, Williams L, Lim A, Martinez M *et al* (2012) Wnt signaling activation in adipose progenitors promotes insulin-independent muscle glucose uptake. *Cell Metab* 15: 492 – 504

Zhan T, Rindtorff N, Boutros M (2017) Wnt signaling in cancer. *Oncogene* 36: 1461 – 1473

